Journal of Medicinal Chemistry

Article

Structure-Permeability Relationship of Semi-Peptidic Macrocycles – Understanding and Optimizing Passive Permeability and Efflux Ratio

Antoine Le Roux, Emilie Blaise, Pierre-Luc Boudreault, Christian Comeau, Annie Doucet, Marilena Giarrusso, Marie-Pierre Collin, Thomas Neubauer, Florian Koelling, Andreas H. Göller, Lea Seep, Dieudonné T Tshitenge, Matthias Wittwer, Maximilian Kullmann, Alexander Hillisch, Joachim Mittendorf, and Éric Marsault

J. Med. Chem., **Just Accepted Manuscript** • DOI: 10.1021/acs.jmedchem.0c00013 • Publication Date (Web): 26 May 2020

Structure-Permeability Relationship of Semi-Peptidic Macrocycles – Understanding and Optimizing Passive Permeability and Efflux Ratio

Antoine Le Roux,[†,‡] Émilie Blaise,[†,‡] Pierre-Luc Boudreault,[†,‡] Christian Comeau,[†] Annie Doucet,[†] Marilena Giarrusso,[†] Marie-Pierre Collin,[$] Thomas Neubauer,[$] Florian Koelling,[$] Andreas H. Goeller,[$] Lea Seep,[$] Dieudonné T. Tshitenge,[$] Matthias Wittwer,[$] Maximilian Kullmann,[$] Alexander Hillisch,[$] Joachim Mittendorf,[$] and Eric Marsault[†,]*

[†] Department of Pharmacology-Physiology and Institut de Pharmacologie de Sherbrooke; 3001, 12[e] av nord ; Sherbrooke (Québec), J1H 5N4.

[$] Bayer AG; Drug Discovery, Pharmaceuticals; D-42096 Wuppertal, Germany.

AUTHOR CONTRIBUTIONS

[‡]ALR, EB and PLB contributed equally to this manuscript.

KEYWORDS.

Macrocycles, semi-peptidic, cellular permeability, structure-permeability relationship, efflux.

ABSTRACT

We herein report the first thorough analysis of the structure-permeability relationship of semi-peptidic macrocycles. In total, 47 macrocycles were synthesized using a hybrid solid phase/solution strategy, then their passive and cellular permeability was assessed using the PAMPA and Caco-2 assay, respectively. Results indicate that semi-peptidic macrocycles generally possess high passive permeability based on the PAMPA assay, yet their cellular permeability is governed by efflux as reported in the Caco-2 assay. Structural variations led to a tractable structure-permeability and structure-efflux relationship, whereby linker length, stereoinversion, *N*-methylation and peptoids site-specifically impact permeability and efflux. Extensive NMR, molecular dynamics and ensemble-based 3D-PSA studies showed that ensemble-based 3D-PSA is a good predictor of passive permeability.

INTRODUCTION

In recent years, macrocycles have generated a lot of interest as scaffolds for drug discovery.[1-5] As a class, they possess the ability to bridge the properties of small molecules, with physicochemical profiles conducive of permeability and oral bioavailability, with those of biologics, characterized by large interacting surfaces suitable for difficult targets such as protein-protein interactions, yet devoid of passive permeability.[6] Marketed macrocyclic drugs (ca 70 in total) largely belong to

natural products and peptides.[3] While natural products, often structurally complex, possess some level of bioavailability to fulfill their natural function, macrocyclic peptides are often poorly permeable and mostly administered parenterally, with the exception of cyclosporine.[3] Owing to their easier synthetic accessibility, potential for diversity and compatibility with chemo-biological methods, the latter are under intense scrutiny. To unlock this class, a major challenge is to guide permeability optimization.[4, 7-13]

Among clinical candidates, designer semi-peptidic macrocycles are a growing subset[3] that can leverage (1) the large diversity of commercially available amino acids, (2) reduced peptidic character and (3) distinct chemical space compared to their fully peptidic congeners.[4, 14, 15] While the structure-permeability of cylic hexa-/heptapeptides and a collection of synthetic macrocycles has been studied,[7, 10, 16-24] semi-peptidic macrocycles have not been systematically studied.

To elucidate the impact of structural features on permeability, we generated 47 derivatives of scaffold **A** (Fig. 1), composed of a tripeptide cyclized head-to-tail with an alkyl linker. The Leu-Ala-Phe peptide was chosen because in NMR the corresponding signals are easily distinguished, making the analysis simpler. Also, the $cLogD_{7.5}$ of the corresponding variations on this scaffold varies between ca 1.5 and 3.5. The impact of discrete structural changes on passive and cellular permeability was assessed using the PAMPA and Caco-2 assays, respectively. Contextually, most permeability studies of cyclic hexapeptides relied on the low efflux MDCK assay, a low efflux cellular passive permeability assay.[7-12] In contrast, this study takes into account both passive and cellular permeability, including efflux as a key component of permeability.

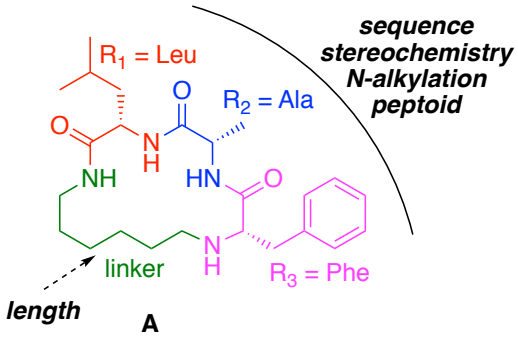

Figure 1. Representative structure of macrocycles in this publication (C6 alkyl linker and (L) stereochemistry shown as examples

RESULTS AND DISCUSSION

Impact of ring size (Table 1) - Analogs were synthesized using a hybrid approach wherein the linear, alkylated tripeptide was assembled on solid phase then macrocyclized in solution (see Experimental Section, Supplementary Scheme S1 and Supplementary Information Procedure 2).[14, 15, 25]

Since size is expected to influence lipophilicity and flexibility,[8, 19, 26, 27] linker length was varied from 2 to 10 atoms (ring sizes 12-20, **1**-**9**). In this series, passive permeability steeply increases with ring size from 12- to 14-membered rings **1**-**3**, with PAMPA -LogP_e ranging from 5.6 to 4.7 (-LogP_e < 6 is considered good permeability, -LogP_e > 7 impermeable, see Supplementary Section 4c for details). A plateau around -LogP_e 4.6 was observed for 14- to 20-membered rings **3**-**9**. In the Caco-2 assay, small macrocycles displayed high efflux and low cellular permeability. The latter increases with ring size and decreasing efflux, with maximal permeability and minimal efflux for 19-membered ring **8**.

Table 1. Influence of ring size on permeability (sequence: Leu-Ala-Phe)

Nr	Linker	Ring size	Caco-2 P_{app} (Efflux)[a]	PAMPA -LogP_e
1	-$(CH_2)_2$	12	4.7 (>20)	5.6

2	$-(CH_2)_3$	13	7.7 (>20)	4.9
3	$-(CH_2)_4$	14	6.4 (>20)	4.7
4	$-(CH_2)_5$	15	19.4 (>20)	4.6
5	$-(CH_2)_6$	16	21.5 (19.0)	4.6
6	$-(CH_2)_7$	17	69.3 (5.2)	4.6
7	$-(CH_2)_8$	18	60.7 (3.2)	4.6
8	$-(CH_2)_9$	19	82.4 (3.3)	4.5
9	$-(CH_2)_{10}$	20	45.1 (6.1)[b]	4.5

[a] P_{app} given in nm/s. Efflux calculated as P_{app} (B-A)/ P_{app} (A-B). [b] 63% recovered.

These first results suggest that passive permeability is high, although cellular permeability appears driven by high efflux. The involvement of P-gp in efflux was confirmed by running the Caco-2 assay in the presence of P-gp inhibitor ivermectin.[28] In these conditions (Suppl. Table T1), **2** and **5** possess P_{app} of 95 and 211 nm/s, with efflux ratios of 2.5 and 1.7, respectively. The impact of ring size, on the other hand, suggests a role for either lipophilicity or flexibility in the interaction with P-gp. Furthermore, flexibility may be a key component to modulate permeability (*aka* chameleonic properties).[29]

To better understand passive permeability on a molecular level, we conducted a series of descriptor-based property calculations and molecular dynamics (MD) simulations on this first subset. Comparison of 3D-PSA of multiple conformers of **1** (-LogP_e 5.6) in chloroform with those of the more flexible compound **5** (-LogP_e 4.6) suggests that the higher rigidity of **1** leads to more exposed polar amide groups not involved in IMBHs. The higher flexibility of **5** enables polar NH-groups to be buried in the macrocycle and a higher degree of shielding of carbonyl groups by the amino acid side chains. Thus, carbonyl groups of **1** are solvent-exposed, increasing 3D-PSA and lowering permeability. In the more flexible **5**, the amide NH groups can form intramolecular H-bonds (IMHBs), lowering 3D-PSA and increasing permeability. The difference in 3D-PSA of **1** vs

5 is about 20Å^2 based on conformational sampling and MD simulations in chloroform. Thus, the permeability cliff between **1** and **5** may be attributed to the higher rigidity of **1** due to its smaller size, leading to higher 3D-PSA.

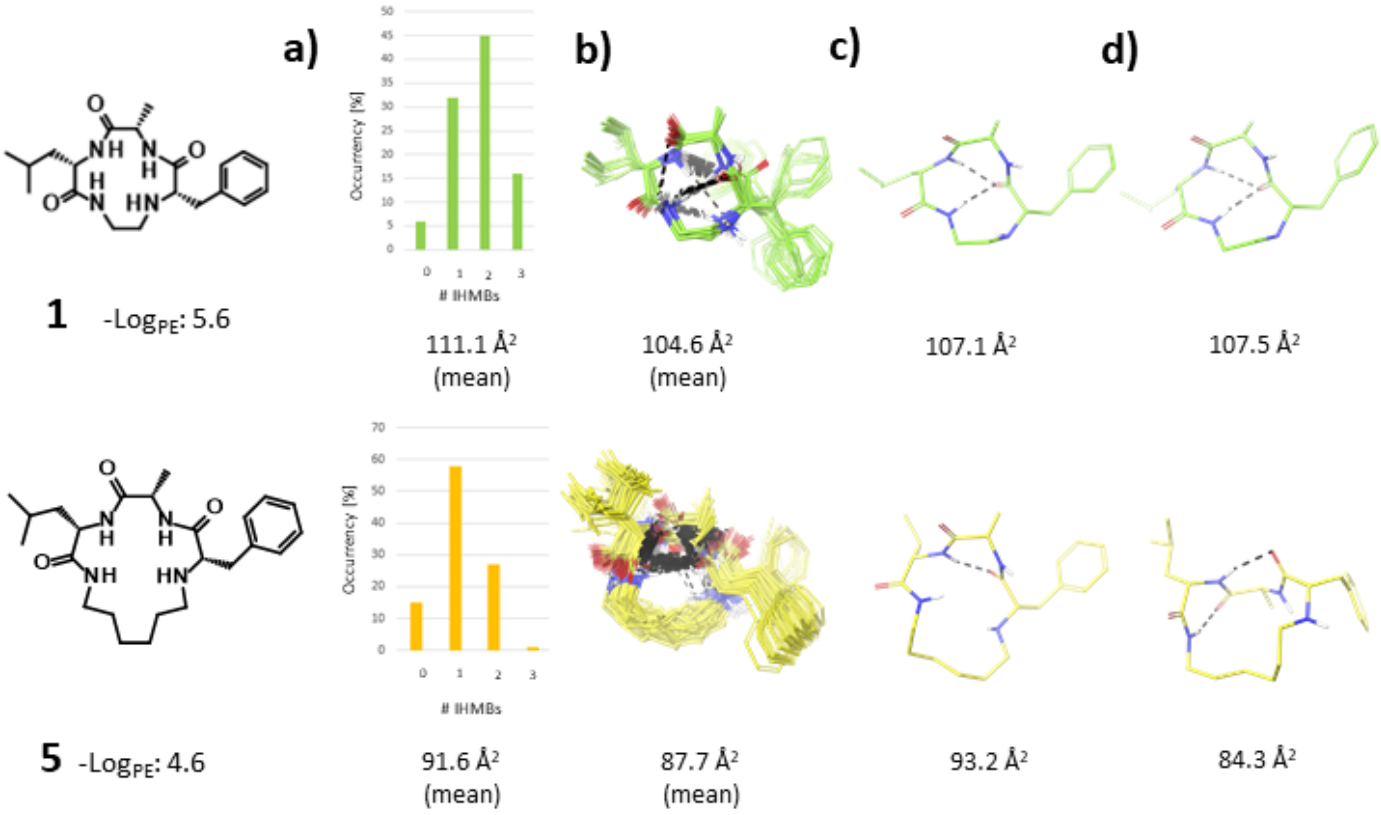

Figure 2. Comparison of different conformations with the corresponding impact on 3D-PSA in CHCl3 for **1** and **5**. a) Intramolecular hydrogen bonds (IHMBs) across 50k MD-snapshots; b) 5 kcal/mol conformer ensemble. c) Representative conformer from b) in good agreement with the mean IHMBs and 3D-PSA compared to a). d) Low Dielectric Conformations (LDCs) demonstrating the tendency to maximize IHMBs.

Impact of peptide sequence (Table 2) - Using **5** as a reference scaffold, the next question was to identify the structural determinants of permeability and efflux. Firstly, sequence permutations, which do not alter calculated 2D properties, marginally influence passive permeability and efflux, which both remain high (PAMPA -LogP$_e$ 4.2 to 4.6 and efflux >18), while cellular permeability remains low to moderate (P$_{app}$ 6 to 21). Notably, Ala in position 3 (i.e., **11**, **12**) leads to poor cellular

permeability, presumably due to the lower ability of the small Ala residue to shield the H-bond donor ability of the adjacent amine.[21]

Table 2. Influence of sequence order on permeability

Nr	Sequence	Caco-2 P_{app} (Efflux)[a]	PAMPA -LogP_e
5	Leu-Ala-Phe-C6	21.5 (18.9)	4.6
10	Ala-Leu-Phe-C6	15.1 (>20)	4.5
11	Leu-Phe-Ala-C6	6.1 (>20)	4.2
12	Phe-Leu-Ala-C6	5.7 (>20)	4.5
13	Ala-Phe-Leu-C6	17.1 (18.6)	4.5
14	Phe-Ala-Leu-C6	12.0 (>20)	4.5

[a] P_{app} given in nm/s. Efflux calculated as P_{app} (B-A)/ P_{app} (A-B).

Impact of stereochemistry (Table 3) - Stereochemistry may impact free energy of desolvation and permeability,[9] depending on side-chain orientation and polarity shielding.[30] Thus, the 8 diastereomers of **5** were synthesized and their permeability measured. Whereas stereoinversion has little impact on passive permeability (PAMPA -LogP_e 4.4 to 4.9), inversion in positions 2 [(D)Ala, **16**] and 3 [(D)Phe, **17**] increases efflux (>20) and decreases cellular permeability (Caco-2 P_{app} 1.4 - 2.1). Conversely, inversion in position 1 [(D)Leu, **15**] reduces efflux while doubling Caco-2 P_{app} (**15** vs **5**, efflux 7.6 vs. 18.9, P_{app} 53.5 vs 21.5). In the presence of ivermectin, the P_{app} of **15** further increases to 420 while its efflux decreases to 0.9 (Suppl. Table T1), confirming that passive cellular permeability remains high. Interestingly also, cellular permeability and efflux mirror in pairs of enantiomers (see **5**, **15**, **16**, **17** vs **21**, **20**, **19**, **18** respectively). This contrasts with results on polar cyclic hexapeptides, which suggested transporter-mediated uptake based on enantiomeric differences.[31] These observations suggest conformational changes and different orientations of the isobutyl side chain of Leu, possibly masking polar backbone atoms.

Table 3. Influence of stereochemistry on permeability

Nr	Sequence	Caco-2 P_{app} (Efflux)[a]	PAMPA -LogP_e
5	Leu-Ala-Phe-C6	21.5 (18.9)	4.6
15	(D)Leu-Ala-Phe-C6	53.5 (7.6)	4.5
16	Leu-(D)Ala-Phe-C6	2.1 (>20)	4.7
17	Leu-Ala-(D)Phe-C6	1.4 (>20)	4.4
18	(D)Leu-(D)Ala-Phe-C6	1.3 (>20)	4.9
19	(D)Leu-Ala-(D)Phe-C6	1.0 (>20)	4.8
20	Leu-(D)Ala-(D)Phe-C6	56.8 (7.8)	4.8
21	(D)Leu-(D)Ala-(D)Phe-C6	13.3 (>20)	4.9

[a] P_{app} given in nm/s. Efflux calculated as P_{app} (B-A)/ P_{app} (A-B).

The impact on efflux is also noteworthy since inversion in position 1 reduces efflux in both enantiomeric series, suggesting a P-gp molecular recognition based on structural pattern rather than individual pharmacophoric elements, congruent with broad specificity.[32]

Impact of *N*-methylation and acetylation (Table 4) - *N*-methylation is beneficial for permeability in cyclic hexa/ heptapeptides when applied site-specifically to solvent-exposed amide bonds.[9, 10, 20, 33] Guidance from NMR analysis was used to rationally optimize the oral bioavailability of a cyclic hexapeptide[20] and an integrin antagonist.[34] Thus, site-selective *N*-methylation and peptoid replacement were implemented on each NH bond (synthesized as per Suppl. Schemes S1, S2).[35]

Table 4. Influence of *N*-methylation and peptoids on permeability

Nr	Sequence	Caco-2 P_{app} (Efflux)[a]	PAMPA LogP_e
5	Leu-Ala-Phe-C6	21.5 (18.9)	4.6
22	Leu(*N*Me)-Ala-Phe-C6	166.9 (2.8)	4.6
23	Gly(*N*iBu)-Ala-Phe-C6	102.0 (3.4)	4.3

24	Leu-Ala(*N*Me)-Phe-C6	14.6 (>20)	4.7
25	Leu-Sar-Phe-C6	2.3 (>20)	4.7
26	Leu-Ala-Phe(*N*Me)-C6	41.6 (7.9)	5.2
27	Leu-Ala-Gly(*N*Bn)-C6	74.1 (4.9)	4.4
28	Leu-Ala-Phe-C6(*N*Me)	43.4 (9.4)	4.3
29	Leu-Ala-Phe(*N*Ac)-C6	11.8 (>20)	5.1

[a] P_{app} given in nm/s. Efflux calculated as P_{app} (B-A)/ P_{app} (A-B).

N-methylation or *N*-acetylation of the secondary amine negatively impact passive permeability (**26**, **29**, -LogP_e > 5). Compared to **5**, *N*-methylation of Leu greatly reduces efflux (18.9 to 2.8) and increases cellular permeability (**22** vs **5**, P_{app} 166.9 vs 21.5 nm/s), while keeping passive permeability unaffected. In the presence of ivermectin, the P_{app} of **22** further increases to 557 with an efflux of 0.67 (Suppl. Table T1). Replacement of Leu by its peptoid (**23**) has a similar effect (efflux 3.4, P_{app} 102.0 nm/s), with marginal increase in passive permeability (**23** vs **5**, -LogP_e 4.3 vs 4.6). In contrast, the same replacements on Ala (**24**, **25**) increases efflux (>20) and reduces cellular permeability (P_{app} 14.6 and 2.3 nm/s), with no impact on passive permeability (-LogP_e 4.7). *N*-methylation or peptoid in position 3 or linker *N*-methylation are beneficial for cellular permeability and efflux (**26**-**28**), yet to a lower extent. Together, inversion of stereochemistry and *N*-methylation/peptoid both influence efflux and cellular permeability site-specifically, with little impact on passive permeability. In agreement with values for PAMPA permeability, a narrow distribution of 3D-PSA values could also be observed (Suppl. Table T2).

A strong tendency to maximize IMHBs in aprotic solvents such as $CHCl_3$ (a surrogate of membrane environment with similar dielectric) is described for larger macrocyclic systems.[19, 36] To understand whether this class behaves similarly, NMR and MD studies were conducted in different solvents to assess the presence of IMHBs and their impact on passive permeability.

IMHBs are expected to lower PSA and grant higher passive permeability.[7d, 7e, 16] Given that stereoinversion or *N*-methylation in position 1 greatly increases permeability, we performed NMR experiments on **5**, **15** and **22** in $CDCl_3$ (hydrophobic) and DMSO (polar), and determined the amide acidity coefficient using experimental shifts in both solvents (*aka* NMR *A* value which gives a 'quantitative' assessment of IMHB, Fig. 3 and Supplementary Figure F1).[37] Amide groups with A < 0.05 are involved in IMHB, while those with A > 0.16 are not.[37] Donor-acceptor pairs for IMHB were further identified by 2D heteronuclear NOE (2D-HOESY) NMR. The results are summarized in Fig. 4. In both experiments, amides D1 and D3 in **22** displayed IMHB with A2, which was the strongest in this series. Stereoinversion in position 1, *i.e.* **15** vs **5**, did not increase IMHBs as observed by NMR.

Empirical difficulties in monitoring 2D-NMR cross-peaks and some variabilities in the spectra suggest a higher flexibility for these molecules in comparison with other published macrocycles such as hexa/heptapeptides.

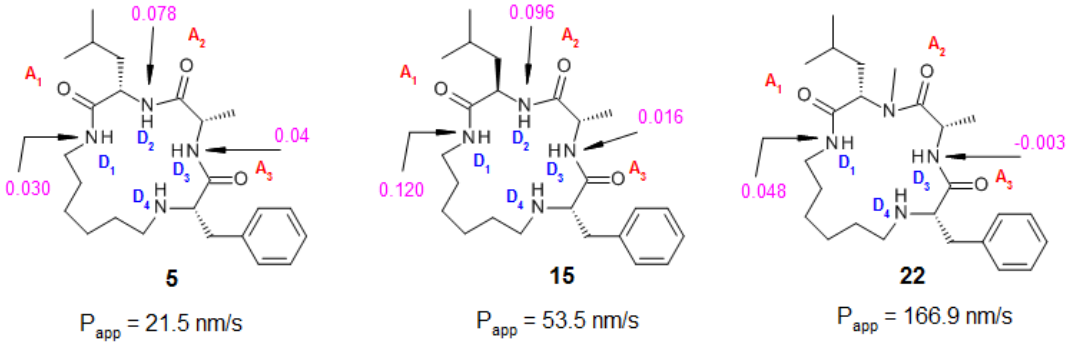

Figure 3. NMR A values of the amide groups for macrocycles **5**, **15** and **22**, determined in DMSO-d_6 and $CDCl_3$, displayed with the potential donor and acceptor positions.

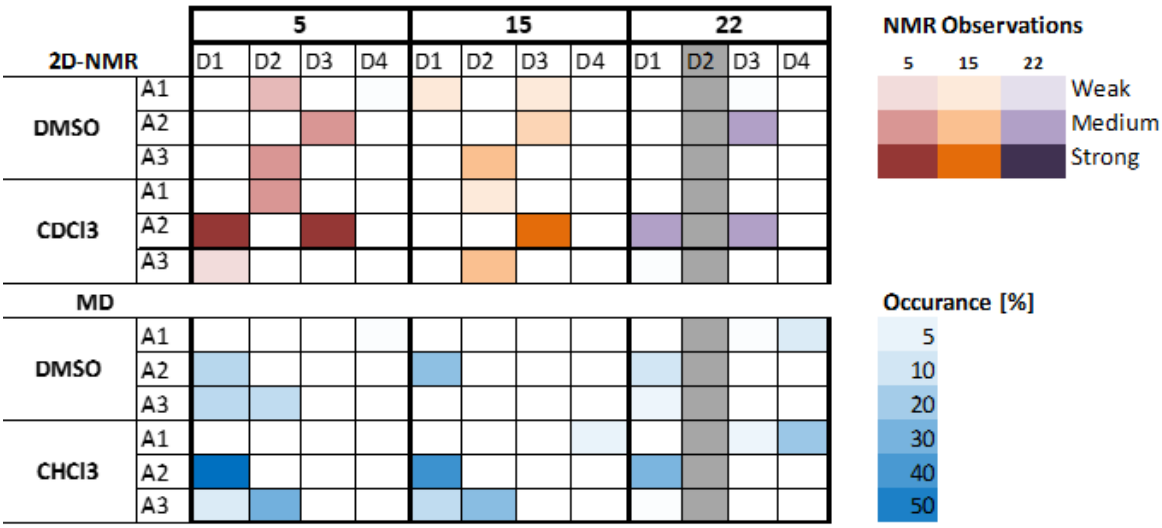

Figure 4. IMHB patterns for macrocycles **5**, **15** and **22** from NMR (top) and MD simulations (bottom), determined in DMSO-d_6 and $CDCl_3$. NMR IMHB patterns are given in classes weak, medium, strong and are quantitative for individual molecules only, whereas MD IMHB patterns are comparable between molecules and given in percentages of snapshots displaying respective IMHB. For compound **22**, D2 was discarded due to N-methylation (grey column).

Extensive molecular dynamics (MD) simulations for seven selected compounds (**1**, **5**, **15**, **24**, **25**, **26**, **28**) in different charge states and solvents were performed using the OPLS3.1 force field.[38] A detailed analysis for **5**, **15** and **22** is shown in Fig. 4 (bottom) to elucidate preferred conformational states and common IMHB patterns. Per molecule, five 100 ns MD simulations were performed at 300 K, starting from five diverse conformers each, both in explicit $CHCl_3$ and DMSO, producing 50,000 snapshots each that were analyzed for IMHB patterns (Figure 4). Generally, probabilities of forming IMHB in DMSO are lower (and even lower for H_2O, data not shown), but there is only weak coincidence with NMR data. Based on MD, D1-A2 for all molecules and D2-A3 for **5** and **15** are the most important IMHB, with occurrences in at least 20% of the snapshots. We assume incomplete or imbalanced sampling or sub-optimal state analysis[39] to account for these differences. Together, both NMR and MD analyses confirm that structural modifications impact IMHB patterns, but with different conclusions. Yet, how these impacts permeability is unclear. These conclusions differ significantly from larger, fully peptidic

macrocycles in terms of IMHB.[19] One possible explanation is that the alkyl linker cannot accommodate strong transannular IMHBs observed in cyclic hexapeptides (which display amide bonds all around the ring), while imparting higher flexibility, which together contribute to prevent a conserved IMHB pattern.

Combining beneficial structural elements (Table 5) - The next question is whether the observed structure-permeability relationship is synergistic. As testified by compounds **30**-**39**, this is generally the case for both cellular permeability and efflux, whereas passive permeability remained invariable. Indeed, analogs **30**, **32**, **34** and **39**, which combine best features at positions 1, 3 and linker, possess very high Caco-2 permeabilities (P_{app} 346.0, 189.3, 270.3 and 266.0 nm/s) and no efflux. Interestingly, *N*-methylation or stereochemical inversion in position 2 reduces permeability, even combined with positive features on other positions (e.g., **31** vs **22**, **33** vs **28**), although this is overweighed by positive features in position 1 (see for example, **37** vs **38)**. Ivermectin has marginal effect on the permeability and efflux of compound **34**, as expected (Suppl. Table T1).

Table 5. Combination of structural modifications

Nr	Sequence	Caco-2 P_{app} (Efflux)[a]	PAMPA -LogP_e
5	Leu-Ala-Phe-C6	21.5 (18.9)	4.6
30	(D)Leu(NMe)-Ala-Phe-C6	346.0 (0.7)	4.6
31	Leu(NMe)-(D)Ala-Phe-C6	38.5 (11.1)	4.6
32	(D)Leu-Ala-Phe-C6(NMe)	189.3 (2.0)	4.7
33	Leu-(D)Ala-Phe-C6(NMe)	7.7 (>20)	4.6
34	(D)Leu(NMe)-Ala-Phe-C6(NMe)	270.3 (0.9)	4.4
35	Leu(NMe)-(D)Ala(NMe)-Phe-C6	207.0 (1.1)	4.6
36	Leu(NMe)-(D)Ala-Phe-C6(NMe)	63.4 (6.4)	4.5
37	Leu(NMe)-(D)Ala(NMe)-Phe-C6(NMe)	200.6 (1.3)	4.5

38	Leu-(D)Ala(NMe)-Phe-C6(NMe)	40.0 (9.9)	4.6
39	Gly(NiBu)-Ala-Phe-C6(NMe)	266.4(1.6)	4.5

[a] P_{app} given in nm/s. Efflux calculated as P_{app} (A-B)/ P_{app} (BA).

Impact of expanding side chain diversity (Table 6) - In order to increase the range of passive permeabilities and explore potential correlations with calculated descriptors, we expanded the dataset via more polar side chains such as Ser or Tyr (compounds **40**-**47**). As expected, the passive permeability of alcohol-containing side chains dropped compared to **5**. In order to understand structure-permeability relationship throughout the entire series, we conducted a series of property calculations.

Table 6. Broader side chain variations

Nr	Sequence	PAMPA -LogP_e
5	Leu-Ala-Phe-C6	4.6
40	Val-(D)Ser-Gly-C6	>7.8
41	Leu-Tyr-Ala-C6	6.7
42	Tyr-Pro-Gly-C6	>7.8
43	Leu-(D)Tyr-Gly-C6	>8.2
44	Leu-(D)Tyr-(D)Ala-C6	6.6
45	Val-(D)Ser-(D)Ala-C6	6.3
46	Ser-(D)Leu-(D)Ala-C6	5.5
47	Tyr-Pro-(D)Ala-C6	> 7.8

Understanding passive permeability on a molecular level: analysis of the entire macrocycle dataset (Figure 5) - Many 3D-permeability prediction models postulate the existence of a low dielectric conformation (LDC) in hydrophobic environment. Key characteristics of the LDC, largely derived from cyclic hexapeptides, are the tendency to maximize IMHBs in combination with a collapsed fold, which shields polarity.[19] This led to the notion of chameleonic properties,

i.e. the ability to modulate conformation and polar surface area as a function of the environment, necessary for beyond-rule of 5 compounds to reach acceptable permeabilities.[29, 40] In contrast to NMR or MD studies, permeability descriptors can be calculated rapidly to enable *in silico* library profiling to support the design of collections with desired physicochemical properties. Several descriptors were used in the past to predict permeability on larger macrocyclic peptides[19, 36] other subclasses of macrocycles,[41] and to predict passive membrane permeability of non-macrocyclic systems. [8, 42, 43]

Accordingly, a selection of descriptors frequently used for permeability predictions was calculated for the broader dataset (i.e. compounds **1**-**47**) and correlated against PAMPA data (Caco-2 permeability was not considered due to the confounding efflux parameter). It is important to point out that the current permeability data do not show a well-balanced and continuous distribution: a majority of compounds show good PAMPA permeability, whereas low permeability is observed only for seven data points (including four left censored measurements with a -$LogP_e$ > 7, which were discarded from regression analysis). Of importance, the dataset covers four -$LogP_e$ units. Table 7 gives a short overview of the selected methods. More descriptors being used for permeability prediction, methods and information on dataset preparation can be found in the supporting information (Table T5), as well as a summary of all calculated properties (Table T6).

Table 7. Descriptors used for correlation with PAMPA permeabilities

Nr	Descriptor Name	Conformation resp. coordinates used	r^2 (r^2)[c]	Ref
4a	cLogD 7.5	2D-Structure	0.41 (0.61)	44, 45
4b	[b]ΔG_{insert}	LDC	0.51	19
4c	[a] 3D-PolarSASA	LDC	0.55	46

4d	[a] 3D-PolarSASA	3D-Conformers in 5 kcal/mol E-Window	0.64 (0.76)	-

[a] Pipeline Pilot Implementation (Version 16.5.0.143 ; http://www.3dsbiovia.com); [b] Maestro (Version 2018-1; www.schrodinger.com); [c] left censored data included for regression in brackets;

Since the PAMPA assay mimics an artificial lipophilic membrane, a good correlation with descriptors encoding lipophilicity could be expected. Surprisingly, $cLogD_{7.5}$ displayed only an r^2 of 0.41 (Fig. 5a). The ΔG_{insert} descriptor claims the existence of a low dielectric conformation (LDC) with a tendency to maximize IMHBs showed only a medium r^2-value of 0.51 (Fig. 5b). As indicated by NMR and MD studies in the underlying scaffold class, no isolated LDC or highly conserved IMHB pattern was identified, possibly explaining these r^2-values. The 3D-PSA calculated on the LDC indicates a slight improvement of 0.55 (Fig. 5c). The use of single LDCs could be problematic, since they tend to form compact conformations with very low 3D-PSA of ~ 40Å^2, which might not reflect reality. To overcome this, 2D structures were converted to 3D using Corina,[47, 48] then submitted for conformational sampling in chloroform with a maximum of 1,000 conformers[48, 49] and a mean 3D-PSA was calculated. Instead of averaging the 3D-PSA across the entire ensemble,[50] only low energy conformers within a 5 kcal/mol energy window using the OPLS3.1 force field[38] were considered. While working on an ensemble-based 3D-PSA, values increased about 20 Å^2 leading to an improved r^2-value of 0.64 (Fig 5d). In contrast to single and static LDC, ensemble-based 3D-PSA recapitulates a hyper-topology that integrates different IMHB patterns and flexibility via a representative number of conformers within 5 kcal/mol.

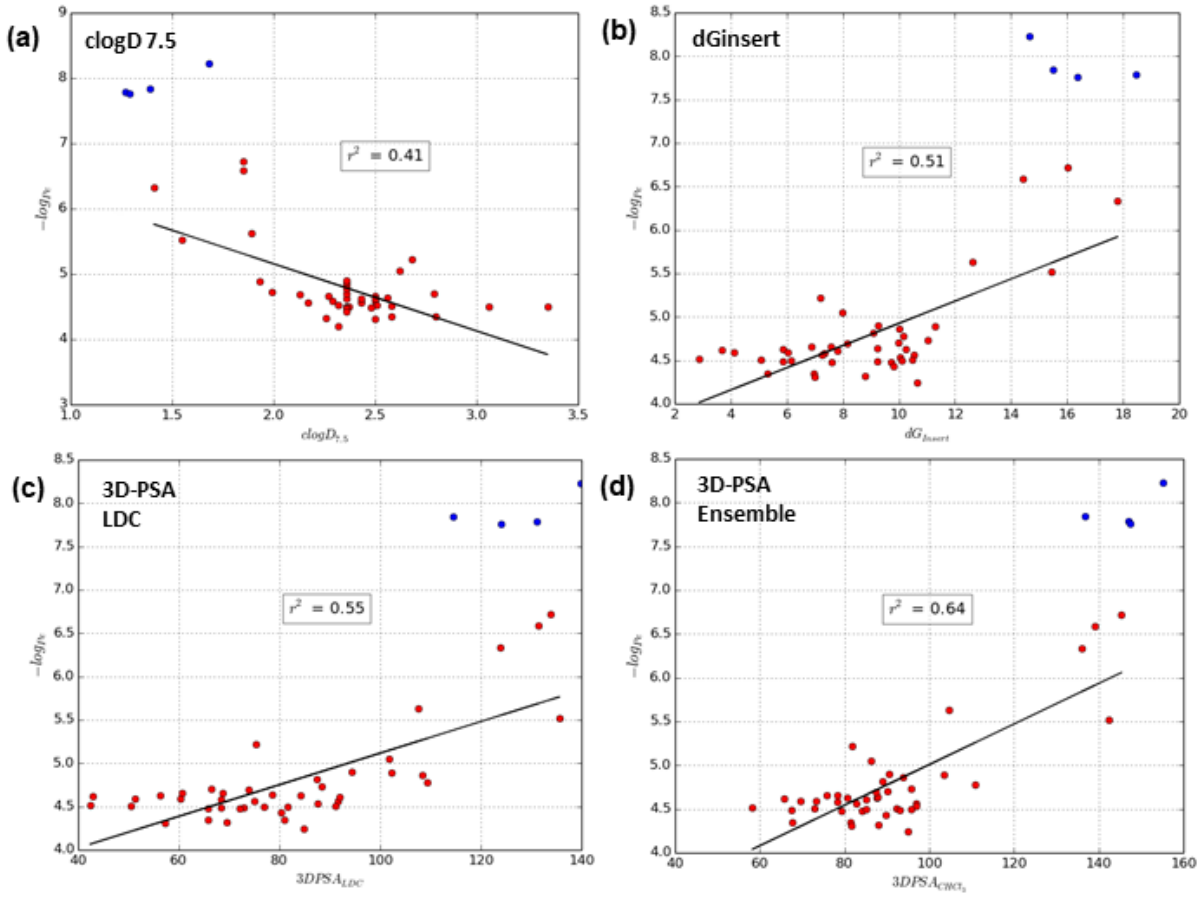

Figure 5 Correlation plots between PAMPA-permeability and selected descriptors. Blue dots represent left censored data points which were discarded from regression analysis.

The impact of such conformational ensemble analysis becomes obvious when comparing the rigid 12-membered ring **1** (-LogP$_e$ 5.6) with the more flexible **5** (-LogP$_e$ 4.6, see Fig. 2). The higher rigidity of **1** prevents transannular orientation of H-bond donors, yet does not necessarily reduce the number of H-bonds. Moreover, carbonyl groups of **1** are more solvent exposed, leading to higher 3D-PSA and lower permeability. Since **5** is more flexible, its 3D-PSA is lower and its permeability higher. Flexibility is also represented by the size of the 5 kcal/mol ensembles which is much smaller for **1** (29 conformers) compared to **5** (100 conformers). The mean 3D-PSA of the 5 kcal/mol ensembles matches the mean 3D-PSA across the 50,000 MD-snapshots very closely. More details can be found in the Suppl. Figures F3, F4 and Suppl. Table T3 and T4). Results of

an extended descriptor set used for PAMPA permeability predictions can be found in (Suppl. Figure F2 and Suppl. Table T5). Finally, there was no correlation between measured solubility and permeability in the PAMPA assay (Suppl. Figure F5).

CONCLUSION

This first study on the structure-permeability of semi-peptidic macrocycles indicates that this class possesses distinct behaviour compared to macrocyclic hexa- and heptapeptides. In contrast to the latter, neither NMR nor MD experiments showed the prevalence of an LDC-conformation maximizing IMHBs, possibly due to their semi-peptidic nature and the presence of a hydrocarbon linker. Indeed, the opportunity for strong IMHBs with an alkyl linker is greatly reduced compared to hexapeptides which feature amide bonds along the whole ring. Moreover, higher rigidity for smaller rings appears detrimental for passive permeability.

The passive permeability of this class is generally high with a narrow distribution. Its cellular permeability ranges from low to very high and is efflux-driven, with significant contribution from P-glycoprotein. Most importantly, while sequence order has little influence on efflux, site-specific stereoinversion, *N*-methylation and peptoids are all highly positive in position 1, detrimental in position 2, and have positive or smaller negative effects in position 3 and the linker. Importantly also, beneficial features are synergistic, offering a tractable structure-permeability relationship.

In terms of molecular descriptors, 3D-PSA demonstrated the best correlation with passive permeability for this scaffold. An ensemble-based 3D-PSA is advantageous in terms of eliminating conformations with very low 3D-PSA, leading to higher r^2-values. In agreement with Whitty and co-workers, we find that a 3D-PSA below 140 $Å^2$ emerges as a reasonable threshold for PAMPA permeability in this scaffold class [29] and might be a reasonable descriptor for other datasets as well.

Moreover, the ensemble-based 3D-PSA matches the mean 3D-PSA across 50,000 MD-snapshots very closely and might be a good alternative for analyzing relevant 3D-conformations in different solvents, while investing far less computational resources.

Finally, the lack of impact of IMHB on permeability is consistent with efflux-driven permeability, suggesting that conformational modulation is an important component of structure-permeability. Overall, this study is the first to provide a detailed analysis of the structure-permeability relationship of semi-peptidic macrocycles, a growing class among development candidates.[3, 51]

EXPERIMENTAL SECTION

Materials. Protected amino acids were purchased from Chem-Impex International (USA). 2-chlorotrityl chloride polystyrene resin was purchased from Matrix Innovation (Canada). All other reagents were purchased from Sigma-Aldrich (Canada) or Fisher Scientific (USA), of the highest commercially available purity, and were used as received.

Peptide synthesis was performed on Silicycle MiniBlocks. Crude peptides were purified by reverse-phase chromatography using a Waters Preparative LC (Sample Manager 2767 (Fraction collector), Binary gradient module 2545, with two 515 HPLC pump and a System Fluidics Organizer SFO, Photodiode Array Detector 2998: column X Select CSH Prep C18 5 μm OBD 19 x 250 mm^2 column, buffer: A: 0.1% HCOOH in H_2O, B: 0.1% HCOOH in ACN, Flow 20 mL/min. Analytical HPLC chromatograms were recorded on a Waters UPLC H-Class with UV detection PDA equipped with an Acquity UPLC CSH C18 1.7μm 2.1 x 50 mm^2 column. MS spectra were recorded on a Waters SQ Detector 2 (electrospray) instrument, with the following gradient conditions: 0 → 0.2 min, 5% acetonitrile; 0.2 → 1.5 min, 5 → 95%; 1.5 → 2 min, 95%. MS spectra

were recorded on a Waters SQ Detector 2 (electrospray) instrument. NMR spectra were recorded on a Bruker Avance III HD 400 MHz and Neo 500 MHz and are reported relative to deuterated solvent signals. Data for ^{1}H NMR are reported as follow: chemical shift (δ ppm), multiplicity (s: singlet, bs: broad singlet, d: doublet, t: triplet, q: quartet, quint: quintet, hex: hexuplet), integration and coupling constant (Hz). ^{13}C NMR spectra were recorded on a Bruker spectrometer at 101 MHz and 126 MHz. Data for ^{13}C NMR are reported in terms of chemical shift (δ ppm). Exact mass measurements were recorded on an electrospray quadrupole time-of-flight Maxis 3G from Bruker using positive mode.

Solid phase synthesis.

NB: number of equivalents are given with respect to nominal resin loading. Typically, 200 mg of resin was used per well, using 24-well Bohdan miniblocks shaken at 600 rpm. Washing times included shaking for 5 min followed by draining. Volumes are given per well.

Procedure 1 - General synthesis scheme for macrocycles with secondary amine on AA3 (Scheme S1, macrocycles 1-25, 28-47)

- *AA1 attachment on 2-chlorotrityl chloride resin*

A solution of Fmoc-AA1-OH (2 eq) and DIPEA (4 eq) in a mixture of DMF/DCM 1/4 (1 mL per 100 mg resin) was added to the resin, and the mixture was shaken for 1h at room temperature. After filtration, the resin was washed five times with DMF (1.25 mL).

- *AA2 and AA3 coupling*

A solution of Fmoc-AA-OH (3 eq) and HATU (3 eq) in DMF (1 mL for 100 mg resin) was added to the resin, followed by DIPEA (4 eq), and the mixture was shaken for 2h at room temperature. After filtration, the resin was washed five times with DMF (1.25 mL).

- *Fmoc cleavage with piperidine (AA1 ≠ N-Alkyl amino acids)*

A solution of 20% piperidine in DMF (1 mL) was added to the resin, and the mixture was shaken for 10 min at room temperature. After filtration, a fresh solution of 20% piperidine in DMF (1 mL) was added, and the mixture was shaken for 10 min at room temperature. After filtration, the mixture was washed five times with DMF (1.25 mL) in the case of the deprotection of AA1, and twice with DMF, once with *i*PrOH, once with DCM, once with *i*PrOH and twice with DCM (1.25 mL each) in the case of AA3.

- *Fmoc removal with DBU (AA1 = N-Alkyl amino acids)*

A solution of 2% DBU in DMF (1 mL) was added to the resin, and the mixture was shaken for 3 min at room temperature. After filtration, a fresh solution of 2% DBU in DMF (1 mL) was added, and the mixture was shaken for 3 min at room temperature. After filtration, the mixture was washed five times with DMF (1.25 mL).

- *AA3 nosylation*

A solution of NsCl (4 eq) and 2,4,6-collidine (10 eq) in NMP (1 mL) was added, and the mixture was shaken for 15 min at room temperature. After filtration, the mixture was washed twice with DMF, once with *i*PrOH, once with DCM, once with *i*PrOH and twice with DCM (each with 1.25 mL).

- *Fukuyama-Mitsunobu linker alkylation*

A solution of Fmoc-protected alcohol (3 eq) and triphenylphosphine (3 eq) in THF (1 mL) was added to the resin, followed by DIAD (3 eq). The mixture was shaken overnight at room temperature. After filtration, the resin was washed twice with DMF, once with *i*PrOH, once with DCM, once with *i*PrOH and twice with DCM (1.25 mL each).

- *Simultaneous Fmoc/nosyl removal*

A solution of *n*-propylamine (10 eq), piperidine (10 eq) and 2,2'-(ethylenedioxy)diethanethiol (10 eq) in DMF (1 mL) was added to the resin, and the mixture was shaken for 1h at room temperature. After filtration, a second identical cycle was repeated. After filtration, the resin was washed twice with DMF, once with *i*PrOH, once with DCM, once with *i*PrOH and twice with DCM (1.25 mL each).

- *Resin cleavage*

A solution of 30% HFIP in DCM (1 ml for 100 mg resin) was added to the resin, and the mixture was shaken for 1h at room temperature. After filtration, the resin was washed with DCM (1.25 mL) and shaken for 3 min, then filtered. The combined DCM phases were concentrated *in vacuo* then dried.

- *Macrocyclization*

The above crude linear compound was dissolved in DMF (final concentration: 0.05M, based on nominal resin loading), then DEPBT (1.1 eq) and DIPEA (3 eq) were added, and the mixture was stirred overnight at room temperature. The mixture was then filtered over a pad of silica-carbonate scavenger (10 eq) and washed with 4 x 2 mL of DMF. The combined DMF phases were concentrated *in vacuo* and dried, then the crude macrocycles were purified by preparative HPLC-MS.

All tested compounds were purified to >95% purity (UPLC-UV-MS) and further characterized by ^{1}H, ^{13}C NMR and HRMS.

SUPPORTING INFORMATION

Supplementary Schemes S1-2, Figures F1-4, Tables T1-7, Smiles structures, Summary of all the calculated properties for macrocycles **1**-**47**. Experimental details (synthetic, biological and computational methods) and full characterization of synthetic intermediates and final compounds can be found in the Supporting Information section of this manuscript.

AUTHOR INFORMATION

Corresponding Author

*Pr Eric Marsault; Institut de Pharmacologie de Sherbrooke; 3001, 12e av nord; Sherbrooke (Qc), Canada J1H 5N4; eric.marsault@usherbrooke.ca

Present Addresses

†If an author's address is different than the one given in the affiliation line, this information may be included here.

AUTHOR CONTRIBUTIONS

The manuscript was written through contributions of all authors. All authors have given approval to the final version of the manuscript. ‡These authors contributed equally.

ACKNOWLEDGMENT

This study was funded by Bayer AG, the Natural Sciences and Engineering Research Council of Canada (RGPIN 2017-05513) and the Canadian Foundation for Innovation.

ABBREVIATIONS

IMHB: IntraMolecular Hydrogen Bonds. LDC: Low Dielectric Constant. MD: Molecular Dynamics. PAMPA: Parallel Artificial membrane Permeability Assay. PSA: Polar Surface Area

REFERENCES

1. Driggers, E. M.; Hale, S. P.; Lee, J.; Terrett, N. K. The Exploration of Macrocycles for Drug Discovery--an Underexploited Structural Class. *Nat Rev Drug Discov* **2008**, 7, 608-624.
2. Marsault, E.; Peterson, M. L. Macrocycles are Great Cycles: Applications, Opportunities and Challenges of Synthetic Macrocycles in Drug Discovery. *J Med Chem* **2011**, 54, 1961-2004.
3. Giordanetto, F.; Kihlberg, J. Macrocyclic Drugs and Clinical Candidates: What can Medicinal Chemists Learn from their Properties? *J Med Chem* **2014**, 57, 278-295.
4. Marsault, E.; Peterson, M. L. Practical Medicinal Chemistry with Macrocycles: Design, Synthesis and Case Studies. Wiley (Hoboken) **2017**.
5. Levin, J. Macrocycles in Drug Discovery. Royal Society of Chemistry (London) **2014**.
6. Cardote, T. A.; Ciulli, A. Cyclic and Macrocyclic Peptides as Chemical Tools to Recognize Protein Surfaces and Probe Protein-Protein Interactions. *ChemMedChem* **2016**, 11, 787-794.
7. Beck, J. G.; Chatterjee, J.; Laufer, B.; Kiran, M. U.; Frank, A. O.; Neubauer, S.; Ovadia, O.; Greenberg, S.; Gilon, C.; Hoffman, A.; Kessler, H. Intestinal Permeability of Cyclic Peptides: Common Key Backbone Motifs Identified. *J Am Chem Soc* **2012**, 134, 12125-12133.
8. Guimaraes, C. R.; Mathiowetz, A. M.; Shalaeva, M.; Goetz, G.; Liras, S. Use of 3D Properties to Characterize Beyond Rule-of-5 Property Space for Passive Permeation. *J Chem Inf Model* **2012**, 52, 882-890.
9. White, T. R.; Renzelman, C. M.; Rand, A. C.; Rezai, T.; McEwen, C. M.; Gelev, V. M.; Turner, R. A.; Linington, R. G.; Leung, S. S.; Kalgutkar, A. S.; Bauman, J. N.; Zhang, Y.; Liras, S.; Price, D. A.; Mathiowetz, A. M.; Jacobson, M. P.; Lokey, R. S. On-resin N-Methylation of Cyclic Peptides for Discovery of Orally Bioavailable Scaffolds. *Nat Chem Biol* **2011**, 7, 810-817.
10. Nielsen, D. S.; Hoang, H. N.; Lohman, R. J.; Hill, T. A.; Lucke, A. J.; Craik, D. J.; Edmonds, D. J.; Griffith, D. A.; Rotter, C. J.; Ruggeri, R. B.; Price, D. A.; Liras, S.; Fairlie, D. P. Improving on Nature: Making a Cyclic Heptapeptide Orally Bioavailable. Angew Chem Int Ed Engl **2014**, 53, 12059-12063.
11. Fouche, M.; Schafer, M.; Berghausen, J.; Desrayaud, S.; Blatter, M.; Piechon, P.; Dix, I.; Martin Garcia, A.; Roth, H. J. Design and Development of a Cyclic Decapeptide Scaffold with Suitable Properties for Bioavailability and Oral Exposure. ChemMedChem **2016**, 11, 1048-1059.
12. Heinis, C. Drug Discovery: Tools and Tules for Macrocycles. *Nat Chem Biol* **2014**, 10, 696-698.
13. Appavoo, S. D.; Kaji, T.; Frost, J. R.; Scully, C. C. G.; Yudin, A. K. Development of Endocyclic Control Elements for Peptide Macrocycles. *J Am Chem Soc* **2018**, 140, 8763-8770.
14. Hoveyda, H. R.; Marsault, E.; Gagnon, R.; Mathieu, A. P.; Vezina, M.; Landry, A.; Wang, Z.; Benakli, K.; Beaubien, S.; Saint-Louis, C.; Brassard, M.; Pinault, J. F.; Ouellet, L.; Bhat, S.; Ramaseshan, M.; Peng, X.; Foucher, L.; Beauchemin, S.; Bherer, P.; Veber, D. F.; Peterson, M. L.; Fraser, G. L. Optimization of the Potency and Pharmacokinetic Properties of a

Macrocyclic Ghrelin Receptor Agonist (Part I): Development of Ulimorelin (TZP-101) from Hit to Clinic. *J Med Chem* **2011**, 54, 8305-8320.
15. Marsault, E.; Hoveyda, H. R.; Gagnon, R.; Peterson, M. L.; Vezina, M.; Saint-Louis, C.; Landry, A.; Pinault, J. F.; Ouellet, L.; Beauchemin, S.; Beaubien, S.; Mathieu, A.; Benakli, K.; Wang, Z.; Brassard, M.; Lonergan, D.; Bilodeau, F.; Ramaseshan, M.; Fortin, N.; Lan, R.; Li, S.; Galaud, F.; Plourde, V.; Champagne, M.; Doucet, A.; Bherer, P.; Gauthier, M.; Olsen, G.; Villeneuve, G.; Bhat, S.; Foucher, L.; Fortin, D.; Peng, X.; Bernard, S.; Drouin, A.; Deziel, R.; Berthiaume, G.; Dory, Y. L.; Fraser, G. L.; Deslongchamps, P. Efficient Parallel Synthesis of Macrocyclic Peptidomimetics. *Bioorg Med Chem Lett* **2008**, 18, 4731-4735.
16. Over, B.; McCarren, P.; Artursson, P.; Foley, M.; Giordanetto, F.; Gronberg, G.; Hilgendorf, C.; Lee, M. D. t.; Matsson, P.; Muncipinto, G.; Pellisson, M.; Perry, M. W.; Svensson, R.; Duvall, J. R.; Kihlberg, J. Impact of Stereospecific Intramolecular Hydrogen Bonding on Cell Permeability and Physicochemical Properties. *J Med Chem* **2014**, 57, 2746-2754.
17. Tamura, K.; Agrios, K. A.; Vander Velde, D.; Aube, J.; Borchardt, R. T. Effect of Stereochemistry on the Transport of Aca-Linked Beta-Turn Peptidomimetics Across a Human Intestinal Cell Line. *Bioorg Med Chem* **1997**, 5, 1859-1866.
18. Naylor, M. R.; Bockus, A. T.; Blanco, M. J.; Lokey, R. S. Cyclic Peptide Natural Products Chart the Frontier of Oral Bioavailability in the Pursuit of Undruggable Targets. *Curr Opin Chem Biol* **2017**, 38, 141-147.
19. Rezai, T.; Bock, J. E.; Zhou, M. V.; Kalyanaraman, C.; Lokey, R. S.; Jacobson, M. P. Conformational Flexibility, Internal Hydrogen Bonding, and Passive Membrane Permeability: Successful In Silico Prediction of the Relative Permeabilities of Cyclic Peptides. *J Am Chem Soc* **2006**, 128, 14073-14080.
20. Wang, C. K.; Northfield, S. E.; Colless, B.; Chaousis, S.; Hamernig, I.; Lohman, R. J.; Nielsen, D. S.; Schroeder, C. I.; Liras, S.; Price, D. A.; Fairlie, D. P.; Craik, D. J. Rational Design and Synthesis of an Orally Bioavailable Peptide Guided by NMR Amide Temperature Coefficients. *Proc Natl Acad Sci USA* **2014**, 111, 17504-17509.
21. Bockus, A. T.; Schwochert, J. A.; Pye, C. R.; Townsend, C. E.; Sok, V.; Bednarek, M. A.; Lokey, R. S. Going Out on a Limb: Delineating The Effects of beta-Branching, N-Methylation, and Side Chain Size on the Passive Permeability, Solubility, and Flexibility of Sanguinamide A Analogues. *J Med Chem* **2015**, 58, 7409-7418.
22. Ono, S.; Naylor, M. R.; Townsend, C. E.; Okumura, C.; Okada, O.; Lokey, R. S. Conformation and Permeability: Cyclic Hexapeptide Diastereomers. *J Chem Inf Model* **2019**, 59, 2952-2963.
23. Witek, J.; Wang, S.; Schroeder, B.; Lingwood, R.; Dounas, A.; Roth, H. J.; Fouche, M.; Blatter, M.; Lemke, O.; Keller, B.; Riniker, S. Rationalization of the Membrane Permeability Differences in a Series of Analogue Cyclic Decapeptides. *J Chem Inf Model* **2019**, 59, 294-308.
24. Hopkins, B. A.; Lee, H.; Ha, S.; Nogle, L.; Sauvagnat, B.; McMinn, S.; Smith, G. F.; Sciammetta, N. Development of a Platform To Enable Efficient Permeability Evaluation of Novel Organo-Peptide Macrocycles. *ACS Med Chem Lett* **2019**, 10, 874-879.
25. Hoveyda, H. R.; Fraser, G. L.; Marsault, E.; Gagnon, R.; Peterson, M. L. Optimization of a macrocyclic ghrelin receptor agonist (part II): development of TZP-102. Practical Medicinal Chemistry with Macrocycles; E. Marsault and M. L. Peterson Eds; Wiley (Hoboken) **2017**.

26. Camenisch, G.; Alsenz, J.; van de Waterbeemd, H.; Folkers, G. Estimation of Permeability by Passive Diffusion Through Caco-2 Cell Monolayers Using the Drugs' Lipophilicity and Molecular Weight. *Eur J Pharm Sci* **1998**, 6, 317-324.
27. Lipinski, C. A. Drug-like Properties and the Causes of Poor Solubility and Poor Permeability. *J Pharmacol Toxicol Methods* **2000**, 44, 235-249.
28. Gnoth, M. J.; Sandmann, S.; Engel, K.; Radtke, M. In Vitro to In Vivo Comparison of the Substrate Characteristics of Sorafenib Tosylate Toward P-Glycoprotein. *Drug Metab Dispos* **2010**, 38, 1341-1346.
29. Whitty, A.; Zhong, M.; Viarengo, L.; Beglov, D.; Hall, D. R.; Vajda, S. Quantifying the Chameleonic Properties of Macrocycles and Other High-Molecular-Weight Drugs. *Drug Discov Today* **2016**, 21, 712-717.
30. Hewitt, W. M.; Leung, S. S.; Pye, C. R.; Ponkey, A. R.; Bednarek, M.; Jacobson, M. P.; Lokey, R. S. Cell-Permeable Cyclic Peptides from Synthetic Libraries Inspired by Natural Products. *J Am Chem Soc* **2015**, 137, 715-721.
31. Marelli, U. K.; Bezencon, J.; Puig, E.; Ernst, B.; Kessler, H. Enantiomeric Cyclic Peptides with Different Caco-2 Permeability Suggest Carrier-Mediated Transport. *Chemistry* **2015**, 21, 8023-8027.
32. Aller, S. G.; Yu, J.; Ward, A.; Weng, Y.; Chittaboina, S.; Zhuo, R.; Harrell, P. M.; Trinh, Y. T.; Zhang, Q.; Urbatsch, I. L.; Chang, G. Structure of P-Glycoprotein Reveals a Molecular Basis for Poly-Specific Drug Binding. *Science* **2009**, 323, 1718-1722.
33. Chatterjee, J.; Rechenmacher, F.; Kessler, H. N-Methylation of Peptides and Proteins: an Important Element for Modulating Biological Functions. *Angew Chem Int Ed Engl* **2013**, 52, 254-269.
34. Weinmuller, M.; Rechenmacher, F.; Kiran Marelli, U.; Reichart, F.; Kapp, T. G.; Rader, A. F. B.; Di Leva, F. S.; Marinelli, L.; Novellino, E.; Munoz-Felix, J. M.; Hodivala-Dilke, K.; Schumacher, A.; Fanous, J.; Gilon, C.; Hoffman, A.; Kessler, H. Overcoming the Lack of Oral Availability of Cyclic Hexapeptides: Design of a Selective and Orally Available Ligand for the Integrin αvβ3. *Angew Chem Int Ed Engl* **2017**, 56, 16405-16409.
35. Schwochert, J.; Turner, R.; Thang, M.; Berkeley, R. F.; Ponkey, A. R.; Rodriguez, K. M.; Leung, S. S.; Khunte, B.; Goetz, G.; Limberakis, C.; Kalgutkar, A. S.; Eng, H.; Shapiro, M. J.; Mathiowetz, A. M.; Price, D. A.; Liras, S.; Jacobson, M. P.; Lokey, R. S. Peptide to Peptoid Substitutions Increase Cell Permeability in Cyclic Hexapeptides. *Org Lett* **2015**, 17, 2928-2931.
36. Rand, A. C.; Leung, S. S.; Eng, H.; Rotter, C. J.; Sharma, R.; Kalgutkar, A. S.; Zhang, Y.; Varma, M. V.; Farley, K. A.; Khunte, B.; Limberakis, C.; Price, D. A.; Liras, S.; Mathiowetz, A. M.; Jacobson, M. P.; Lokey, R. S. Optimizing PK Properties of Cyclic Peptides: the Effect of Side-Chain Substitutions on Permeability and Clearance. *Medchemcomm* **2012**, 3, 1282-1289.
37. Abraham, M. H.; Abraham, R. J.; Acree, W. E., Jr.; Aliev, A. E.; Leo, A. J.; Whaley, W. L. An NMR Method for the Quantitative Assessment of Intramolecular Hydrogen Bonding; Application to Physicochemical, Environmental, and Biochemical Properties. *J Org Chem* **2014**, 79, 11075-11083.
38. Harder, E.; Damm, W.; Maple, J.; Wu, C.; Reboul, M.; Xiang, J. Y.; Wang, L.; Lupyan, D.; Dahlgren, M. K.; Knight, J. L.; Kaus, J. W.; Cerutti, D. S.; Krilov, G.; Jorgensen, W. L.; Abel, R.; Friesner, R. A. OPLS3: A Force Field Providing Broad Coverage of Drug-like Small Molecules and Proteins. *J Chem Theory Comput* **2016**, 12, 281-296.

39. Prinz, J. H.; Wu, H.; Sarich, M.; Keller, B.; Senne, M.; Held, M.; Chodera, J. D.; Schutte, C.; Noe, F. Markov Models of Molecular Kinetics: Generation and Validation. J Chem Phys **2011**, 134, 174105/1-174105-23.
40. Escalera, J. B.; Bustamante, P.; Martin, A. Predicting the Solubility of Drugs in Solvent Mixtures: Multiple Solubility Maxima and the Chameleonic Effect. *J Pharm Pharmacol* **1994**, 46, 172-176.
41. Over, B.; Matsson, P.; Tyrchan, C.; Artursson, P.; Doak, B. C.; Foley, M. A.; Hilgendorf, C.; Johnston, S. E.; Lee, M. D. t.; Lewis, R. J.; McCarren, P.; Muncipinto, G.; Norinder, U.; Perry, M. W.; Duvall, J. R.; Kihlberg, J. Structural and Conformational Determinants of Macrocycle Cell Permeability. *Nat Chem Biol* **2016**, 12, 1065-1074.
42. Leung, S. S.; Mijalkovic, J.; Borrelli, K.; Jacobson, M. P. Testing Physical Models of Passive Membrane Permeation. *J Chem Inf Model* **2012**, 52, 1621-1636.
43. Kansy, M. F., H.; Kratzat, K.; Wagner, B.; Parrilla, I. High Throughput Artificial Membrane Permeability Studies in Early Lead Discovery and Development. Pharmacokinetic Optimization in Drug Research: Biological, Physicochemical and Computational Strategies; B. Testa; H. van de Waterbeemd; G. Folkers; R. Guy Eds; Verlag Helvetica Chimica Acta, Postfach (Switzerland) **2001**.
44. Hillisch, A.; Heinrich, N.; Wild, H. Computational Chemistry in the Pharmaceutical Industry: From Childhood to Adolescence. *ChemMedChem* **2015**, 10, 1958-1962.
45. Montanari, F.; Kuhnke, L.; Ter Laak, A.; Clevert, D. A. Modeling Physico-Chemical ADMET Endpoints with Multitask Graph Convolutional Networks. *Molecules* **2019**, 25, 1-13.
46. Stanton, D. T.; Jurs, P. C. Development and Use of Charged Partial Surface Area Structural Descriptors in Computer-Assisted Quantitative Structure-Property Relationship Studies. *Anal. Chem.* **1990**, 61, 2323-2329.
47. http://www.3dsbiovia.com. (Accessed Dec. 20, 2019)
48. 3D Structure Generator CORINA Classic, Molecular Networks GmbH, Nuremberg, Germany, www.mn-am.com.
49. Sindhikara, D.; Spronk, S. A.; Day, T.; Borrelli, K.; Cheney, D. L.; Posy, S. L. Improving Accuracy, Diversity, and Speed with Prime Macrocycle Conformational Sampling. *J Chem Inf Model* **2017**, 57, 1881-1894.
50. Krarup, L. H.; Christensen, I. T.; Hovgaard, L.; Frokjaer, S. Predicting Drug Absorption from Molecular Surface Properties Based on Molecular Dynamics Simulations. *Pharm Res* **1998**, 15, 972-978.
51. Qvit, N.; Rubin, S. J. S.; Urban, T. J.; Mochly-Rosen, D.; Gross, E. R. Peptidomimetic Therapeutics: Scientific Approaches and Opportunities. *Drug Discov Today* **2017**, 22, 454-462.

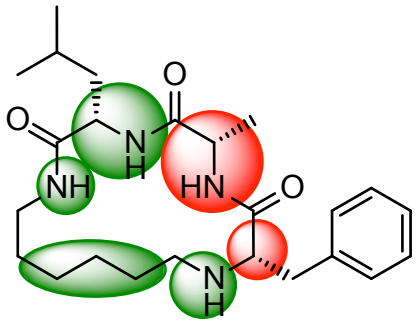
O
O
N
H
NH
HN
O
N
H